Facile synthesis of Cu2SnS3 thin films grown by SILAR method: effect of film thickness

Article *in* Journal of Materials Science: Materials in Electronics · June 2017

DOI: 10.1007/s10854-017-6492-7

J Mater Sci: Mater Electron (2017) 28:7912–7921
DOI 10.1007/s10854-017-6492-7

Facile synthesis of Cu_2SnS_3 thin films grown by SILAR method: effect of film thickness

Harshad D. Shelke[1] · Abhishek C. Lokhande[2] · Vanita S. Raut[1] · Amar M. Patil[1] · Jin H. Kim[2] · Chandrakant D. Lokhande[1,3]

Received: 23 November 2016 / Accepted: 30 January 2017 / Published online: 19 March 2017

Abstract Ternary Cu–Sn–S system, Cu_2SnS_3 (CTS) thin films have been successfully deposited via successive ionic layer adsorption and reaction (SILAR) method. The effect of film thickness on the structural, morphological, wettability and optical properties of CTS material is studied. The XRD studies confirm formation of triclinic (mohite) phase of CTS material. The SEM images show that entire film surface is covered by compact nearly spherical grains over growth of spongy clusters. The Brunauer-Emmett-Teller (BET) analysis revealed that the surface area of CTS material is 2.11 m^2 g^{-1}. The wettability study indicates hydrophilic nature of CTS samples. The optical band gap is decreased from 1.36 to 0.98 eV with increase in film thickness. The photoelectrochemical (PEC) study of CTS material shows anodic photocurrent indicating P-type electrical conductivity.

1 Introduction

In recent years, there is a great deal of interest in research of chalcopyrite semiconductors due to their suitable band gaps and high optical absorption coefficients for potential application in thin film solar cells [1]. Recently, power conversion efficiencies (PCE) of solar cells based on Cu_2ZnSnS_4 (CZTS) and $Cu_2ZnSnSe_4$ (CZTSe) as high as 8.4 and 10.1%, respectively have been reported [2, 3]. The copper based multinary compound semiconductor materials are used as absorber materials in photovoltaic technology. Also, in recent years, importance is given to nontoxic semiconductors from both the fundamental and technological point of view for solar cell materials. Ternary semiconductors such as Cu–Sn–S (CTS) belonging to I–IV–VI groups are preferred as excellent absorber material due to high absorption coefficient (>10^4 cm^{-1}) and small band gap (0.9–1.5 eV) for photovoltaic cells, and as a suitable candidate for nonlinear optical materials. In the Cu–Sn–S system, several ternary compounds including Cu_2SnS_3, Cu_3SnS_4, Cu_4SnS_4, $Cu_2Sn_3S_7$ and $Cu_5Sn_2S_7$ have been previously studied for photovoltaic absorbers. Among them, Cu_2SnS_3 phase shows good performance in photovoltaic device because of its wide stability range and lack of Fermi level pinning [4]. Furthermore, this material offers outstanding optical, thermal and mechanical properties [5].

The Cu_2SnS_3 has been synthesized by both physical and chemical methods. Physical methods include sputtering [6], electron beam evaporation [7, 8], co-evaporation [9, 10], vacuum evaporation [11], solid state reaction [12] and PLD (pulsed laser deposition) [13, 14]. In physical methods, Nakashima et al. [15] reported highest 4.69% PCE by sequential evaporation of NaF/Cu/Sn stacked precursor and Kanai et al. [16] reported 3.66% PCE by co-evaporation method. The CTS thin film are deposited using various chemical methods such as chemical bath deposition (CBD) [17], spin coating [18], hydrothermal [19], electrodeposition [20], successive ionic layer adsorption and reaction

✉ Jin H. Kim
jinhyeok@chonnam.ac.kr

✉ Chandrakant D. Lokhande
l_chandrakant@yahoo.com

[1] Thin Film Physics Laboratory, Department of Physics, Shivaji University, Kolhapur, Maharashtra 416 004, India

[2] Optoelectronic Convergence Research Centre, Department of Materials Science and Engineering, Chonnam National University, Gwangju 500-757, South Korea

[3] Centre for Interdisciplinary Research, D. Y. Patil University, Kolhapur, Maharashtra 416 006, India

(SILAR) [21], spray pyrolysis [22], hot injection [23], solvothermal [24] etc.

Compared to other chemicals methods, SILAR is a simple, less expensive and less time consuming method for the deposition of semiconducting thin films. It is also relevant in the deposition of large area thin films. In SILAR method, substrate is successively dipped into the precursor solution during the deposition process. In this method, deposition cycles and dipping time are important parameters for synthesis of nanoparticles to coating films. Sufficient reaction time favors the complete chemical reaction and hence produces pure phase compounds without secondary phases.

The characteristics of films and their potential applications are interrelated to the crystallinity, surface morphology, grain boundary and grain size, which are affected by the film thickness. For applications in optoelectronic devices technology, the optimum film thickness is preferred for the best device quality and performance. Hence, it is necessary to study the effect of film thickness on the properties of CTS thin films. In present study, by varying the number of deposition cycles, the thickness of CTS film is varied using optimized deposition condition and the effect of CTS film thickness on structural, morphological, wettability, optical and photoelectrochemical properties is studied.

2 Experimental details

All CTS films are deposited on stainless steel (SS) substrates. The SS substrates are polished by zero grade polish paper, ultrasonically cleaned in double distilled water (DDW) for 15 min and then washed by acetone. In a typical synthesis of Cu_2SnS_3, the mixed solution of copper chloride ($CuCl_2{\cdot}2H_2O$), tin chloride ($SnCl_2{\cdot}2H_2O$) and Na_2EDTA ($C_{10}H_{14}N_2Na_2O_8$) is used as the cationic precursor and sodium sulphide ($Na_2S{\cdot}xH_2O$) solution is used as an anionic precursor. Ethylenediaminetetraacetic acid disodium salt (Na_2EDTA) solution is used as a complexing agent who binds metal cation in the solution. The molar concentrations of $CuCl_2{\cdot}2H_2O$, $SnCl_2{\cdot}2H_2O$ and $Na_2S{\cdot}xH_2O$ in the solution are 0.1, 0.05 and 0.2 M, respectively. In the SILAR method, the substrate is immersed into separate cationic and anionic precursor solutions for the adsorption and reaction, and then rinsed with DDW after each immersion to remove the loosely bound particles and to avoid the precipitation. By repeating the cycle described above, CTS thin film with the desired thickness is obtained by adjusting the preparative parameters The deposition of CTS thin films taken at 20, 40 and 60 SILAR cycles are denoted as CTS-20, CTS-40 and CTS-60, respectively. These films are annealed at 300 °C in a vacuum to improve the crystallinity. The CTS films are well adherent, uniform and blackish in color.

3 Materials characterization

To investigate the effect film thickness on the characteristic parameters of the CTS thin films by XRD (X-ray diffraction), Raman spectroscopy, EDAX (Energy dispersive X-ray spectroscopy), XPS (X-ray photoelectron spectroscopy), SEM (scanning electron microscopy), optical absorption, wettability and BET (Brunauer-Emmett-Teller) characterization techniques is used. The thickness of CTS films is measured by Ambios XP-1 surface profiler. The XRD patterns is recorded by a BRUKER AXS D8 Advanced model X-ray diffractometer equipped with Cu radiation (K_α of $\lambda = 1.54$ Å). The Raman spectra of the CTS nanoparticles are trace in the range of 150–500 cm^{-1} using a micro-Raman spectrometer (Via Reflex UV Raman microscope, Renishaw, U.K. at KBSI Gwangju center) use a He–Ne laser source with an excitation wavelength of 488 nm and a resolution of 1 cm^{-1} at 15 mW laser power. The XPS analysis is studied by using VG Multilab 2000, Thermo VG Scientific, UK, for state confirmation of CTS material. The morphology of the samples is analyzed by SEM (JEOL JSM-6390). Optical band gap is determined by the UV–Visible absorption spectroscopy analysis carried out by a HITACHI UV4100 spectrometer. The specific surface area and pore size distribution of CTS powder is studied by BET as well as Barrett-Joyner-Halenda (BJH) analysis using Quantachrome Instruments v11.02 model.

4 Results and discussion

4.1 CTS film formation and reaction mechanism

A schematic explanation of a single cycle for the deposition of CTS film is given in Fig. 1. In CTS thin film formation, ion-by-ion type of deposition occurs via nucleation sites on the adsorbed surfaces [25]. Nucleation takes place as a result of the surface condensation of these ions and results in a dense adherent thin film [26]. The substrate is immersed into the cationic bath precursor, contains mixed $CuCl_2$ and $SnCl_2$ solutions. In the chloride precursors ($CuCl_2{\cdot}2H_2O$ and $SnCl_2{\cdot}2H_2O$), Cu^{2+} and Sn^{2+} species are easily available in the solution. The most stable oxidation state of tin is Sn^{4+}. However, in present work tin contains Sn^{2+} state in $SnCl_2$ compound. In cationic solution bath, Cu^{2+} reduces to Cu^{+} and Sn^{2+} is oxidized to Sn^{4+}. This is best shown in the fact that Sn^{2+} ion in solution is good reducing agents.

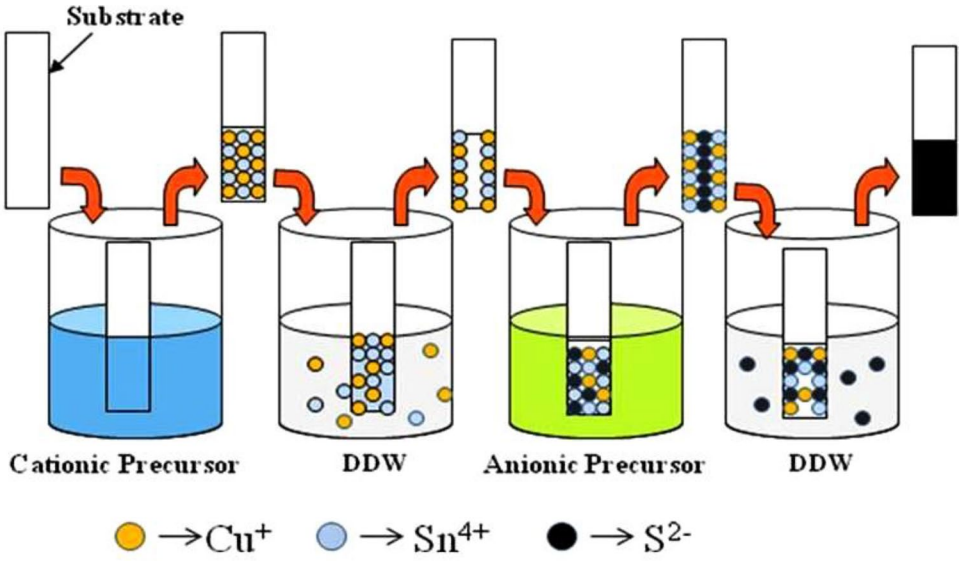

Fig. 1 Schematic of synthesis of CTS thin films by SILAR method

$$2CuCl_2 + SnCl_2 + 6H_2O = 2Cu^+ + Sn^{4+} + 6HCl + 6OH^- \quad (1)$$

After that, substrate is rinsed with DDW to remove the loosely bounded reactants. The anionic precursor bath contains $Na_2S{\cdot}xH_2O$ solution, which gives sulfide ions (S^{2-}) as per following reaction [27].

$$Na_2S + H_2O \rightarrow 2Na^+ + HS^- + OH^- \quad (2)$$

$$HS^- + H_2O \rightarrow H_3O^+ + S^{2-} \quad (3)$$

Finally, the reaction takes place between the pre-adsorbed Cu^{1+}, Sn^{4+} cations and the S^{2-} anion to form a solid CTS thin film as,

$$2Cu^+ + Sn^{4+} + 3S^{2-} \rightarrow Cu_2SnS_3 \quad (4)$$

4.2 Thickness measurement

The variation of film thickness with deposition cycles for CTS films is shown in Fig. 2a. Thickness of CTS thin films is estimated to be 0.526, 0.806, and 1.006 μm for CTS-20, CTS-40 and CTS-60 thin films, respectively and is shown as inset. It is observed from Fig. 2a, that thickness of CTS film increases with deposition cycles. Ideally, in SILAR process, only a single layer of film material is deposited on the substrate in one cycle of deposition. As the deposition cycles continue, more and more layers of the film material are deposited and hence the overall thickness of

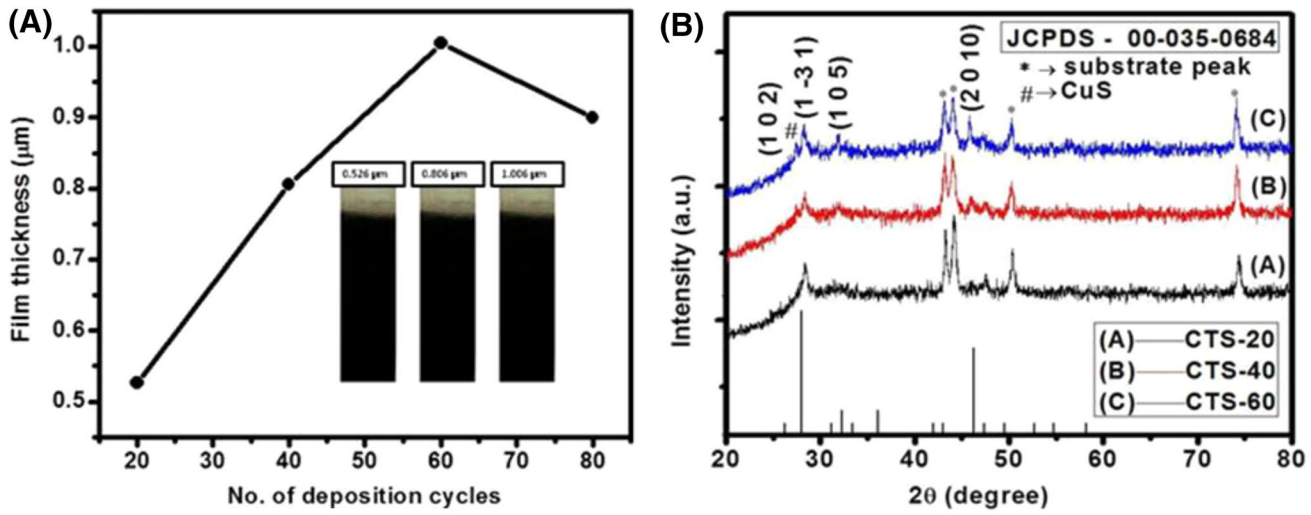

Fig. 2 **a** Plot of thickness variation of CTS thin films with SILAR cycles and **b** XRD patterns of *A* CTS-20, *B* CTS-40 and *C* CTS-60 CTS thin films

the film increases. This may be due to enough reaction time periods available for the formation of CTS thin film. The rate of film thickness is nonlinear which indicates that the growth is due to nucleation and coalescence process. Furthermore, after 60 cycles, slight decrease in CTS film thickness is observed. The reduction in CTS film thickness may due to the development of stress, resulting peel out the film after reaching beyond optimum thickness. The peeling of film material is common in chemically deposited films and is mainly due to the relatively poor adhesion [28]. Thus, the terminal thickness of CTS thin film is 1.006 μm for 60 cycles.

4.3 Structural study

The X-ray diffraction patterns of SILAR deposited CTS thin films with 0.526, 0.806 and 1.006 μm thicknesses are indicated by (A) CTS-20, (B) CTS-40 and (C) CTS-60, respectively in Fig. 2b. It is clear from XRD patterns that CTS films exhibit polycrystalline nature. The presence of peaks at 2θ = 28.49, 32.86 and 47.36° corresponding to diffraction planes of (1–31), (105) and (2010) respectively, indicates the formation of triclinic (JCPDS 00-035-0684) crystal structure of Cu_2SnS_3 material. The relative peak intensity of (105) and (2010) planes enhance with increasing film thickness. The enhanced crystallinity of the films can be attributed to the rearranging of the atoms and removal of defects due to the layer by layer deposition in SILAR method. Ashith et al. [29] reported the similar result of an increase in film crystallinity with increasing film thickness for SILAR deposited CdS thin films. Apart from CTS XRD peaks, additional peak corresponding to secondary CuS phase (indicated by #) is observed in the diffraction pattern. It is clear that the sample is multi-phase containing CuS and Cu_2SnS_3 (JCPDS card no. 035–0684) with triclinic structure, in which CuS is the secondary phase as indicated by the intense (102) peak. The SS substrate peak in the XRD spectra is indicated by asterisk (*) sign. The particle size is estimated using Scherrer's formula

$$D = \frac{0.9\ \lambda}{\beta \cos\theta} \tag{5}$$

where, β is the full width at half maximum intensity (radians) and λ = 1.54 Å is the wavelength of the K_α—X-ray. The particle size is found to be 12 nm for high intense peak (1–31) of CTS-60 thin film.

4.4 Raman spectroscopy

Raman spectroscopy was used as a complementary technique to identify the presence of secondary phases in CTS thin film. Figure 3a indicates the Raman spectra of the CTS thin films. The existence of peaks at 320 and 287 cm^{-1} indicate the formation of CTS with triclinic phase. Also in all the three spectra, secondary phase peaks of CuS (249 and 470 cm^{-1}) and SnS (223 cm^{-1}) are observed. The presence of these secondary phases is attributed due to the difference in the reactivity of the cationic precursors. According to the principle of hard and soft acids and bases (HSAB), soft Lewis base (S) reacts preferentially with soft Lewis acid (Cu) than hard Lewis acid (Sn) leading to the formation of major CuS and minor SnS secondary phase [30]. Thus, Raman study confirms the formation of CTS compound with secondary CuS and SnS phases.

4.5 Energy dispersive X-ray analysis (EDAX)

The elemental study of the CTS thin films deposited at different deposition cycles on SS substrate are carried out by energy dispersive X-ray analysis (EDAX) technique. The respective EDAX spectra are shown in Fig. 3b–d. EDAX examination implies the presence of copper, tin and sulfur for all the samples deposited at various deposition cycles. The stoichiometric ratio of Cu, Sn and S were determined by integrating the region under each Cu, Sn and S peak. Atomic percentage of Cu, Sn and S in CTS thin films for different thickness and the corresponding standard values are shown in Table 1. The chemical composition of the films presented in Table 1 indicates the presence of Cu, Sn and S in stoichiometric amount with slightly copper rich content (Cu/Sn = 2.17–2.49).

4.6 X-ray photoelectron spectroscopy (XPS)

The XPS is a surface responsive quantitative spectroscopic technique that measures the elemental composition, empirical formula, chemical state and electronic state of the elements that are present within a material. The XPS survey spectrum of CTS-60 thin film is shown in Fig. 4a. From XPS spectroscopy, it is clear that CTS material consists of the Cu^{1+}, Sn^{4+} and S^{2-} elements with the quantification of Cu2p, Sn3d and S2p core levels peaks, respectively [31]. The Cu2p, Sn3d and S2p core-level photoelectron spectra with the fitting profile for quantitative elemental composition determination are shown in Fig. 4b–d, respectively. The binding energy of Cu $2p_{3/2}$ and Cu $2p_{1/2}$ peaks are 932.77 and 952.50 eV, respectively [32]. The satellite peaks does not observed around 932 and 955 eV at Cu2p core level, which represents the existence of copper is Cu^{1+} state in CTS material [33]. The binding energies for Sn $3d_{5/2}$, Sn $3d_{3/2}$ and S $2p_{3/2}$ are 487.15, 495.61 and 163.36 eV, respectively, which match well with the earlier reports [34, 35]. The

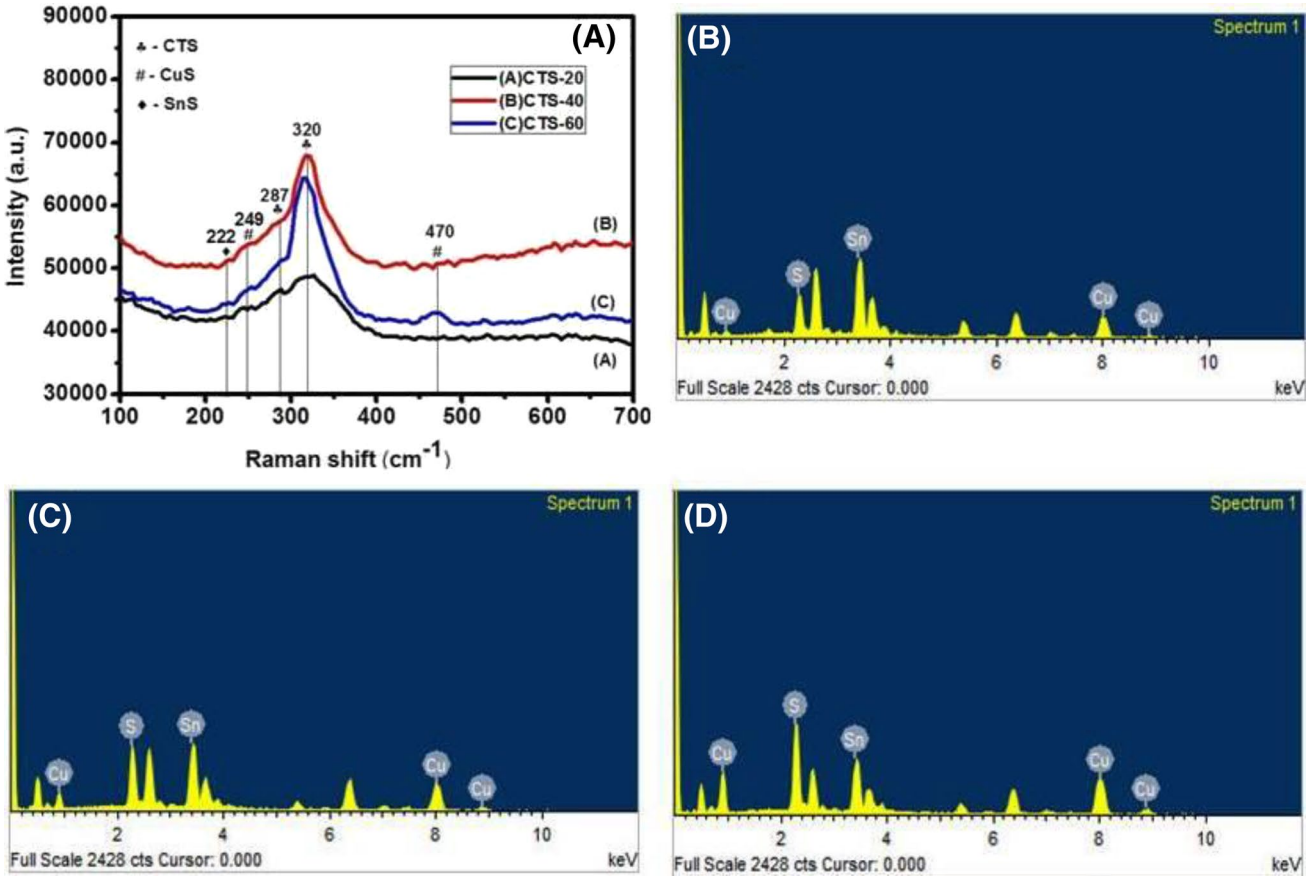

Fig. 3 **a** Raman analyse of CTS thin films and Energy dispersive X-ray spectroscopy (EDAX) of **b** CTS-20, **c** CTS-40 and **d** CTS-60 thin film

Table 1 Atomic percentage of Cu, Sn and S in Cu_2SnS_3 thin films

Sample	Thickness (μm)	Cu at.%	Sn at.%	S at.%	Cu/Sn
CTS-20	0.526	29.31	13.5	54.79	2.17
CTS-40	0.806	30.40	13.1	56.5	2.32
CTS-60	1.006	31.71	12.7	57.99	2.49

XPS confirms presence of Cu and Sn in +1 and +4 oxidation states, respectively.

4.7 SEM analysis

Figure 5a–f shows SEM images of CTS films with thickness of (a, b) 0.526 μm, (c, d) 0.806 μm and (e, f) 1.006 μm for 20, 40 and 60 deposition cycles, respectively at 5000 and ×20,000 magnifications. An increasing number of SILAR deposition cycles show significant change in surface morphology of CTS thin films. Figure 5a, b shows a non-uniform distribution of agglomerated nanocrystals i.e. it shows the incomplete crystal growth over the entire surface of substrate. It does not exhibit appreciable grain formation. The grain formation is seen in Fig. 5c, d. The uniform density, adhesion to the substrate and compact nature of the film increased with film thickness. With increase in deposition cycles, enhancement is agglomeration of the grains and compactness of the film, results in the formation of cluster type structure. SEM images in Fig. 5e, f indicate that CTS film is composed of a dense packing of grains without any voids, signifying uniformity and compact nature of thin film surface. Also, a small crystallites growth on compact surface is observed. Further with increase in deposition cycles, film surface becomes deteriorated and slight decrease in film thickness is observed. Jadhav et al. [36] has reported deterioration in SILAR deposited films, while Salgam et al. [37] observed macroscopic defects such as voids and cracks on the surface of the film with thickness.

4.8 BET analysis

The PEC cell performance of the active electrode material is mainly dependent on the surface conditions. The surface area plays an important role in solar cells for light absorption at different incident angles. So, it is important to carry out BET analysis for CTS material. In order to indicate

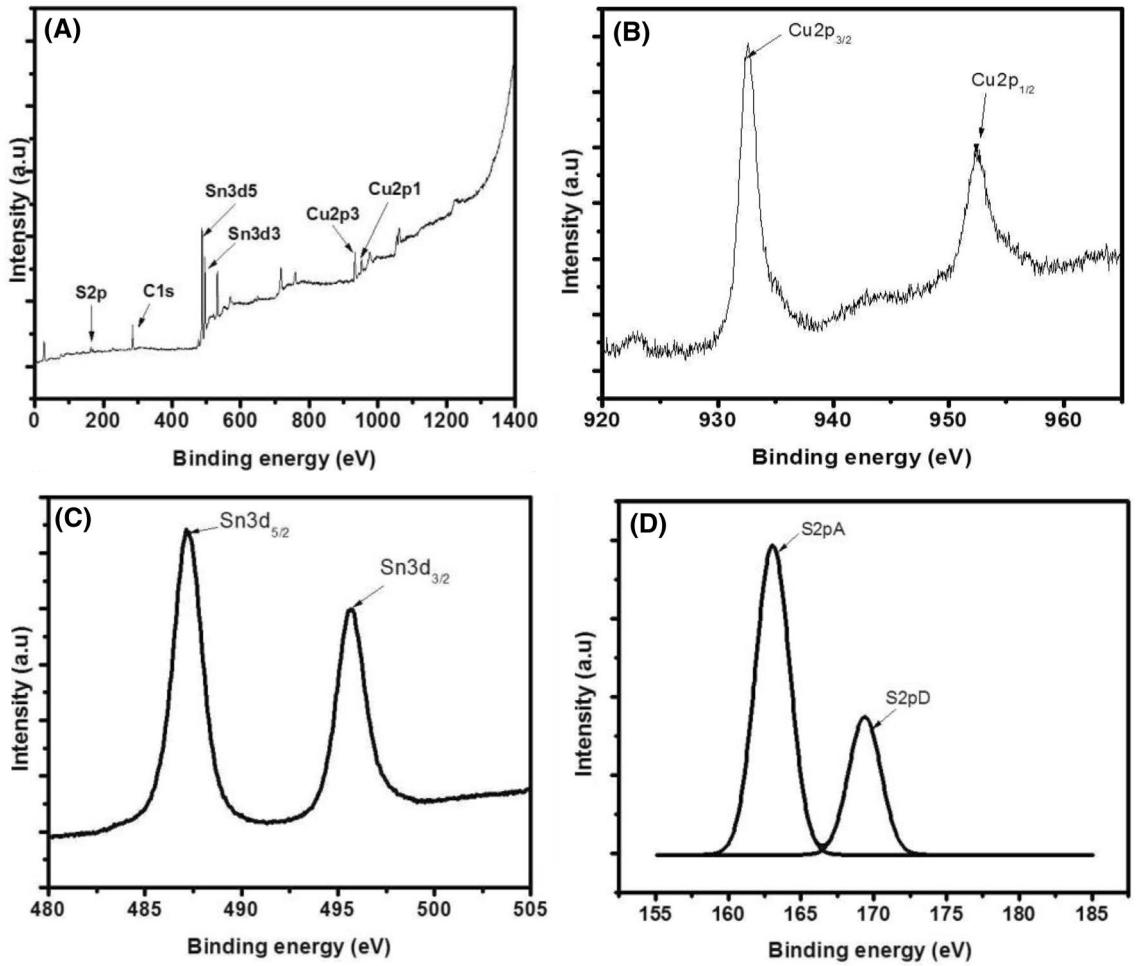

Fig. 4 X-ray photoelectron spectra of CTS material. **a** Survey spectrum, **b** Cu 2p core level, **c** Sn 3d core level and **d** S 2p core level

the compactness of CTS material, N_2 adsorption–desorption isotherms are measured for powder sample of CTS-60 thin film scratched from the corresponding electrode (see Fig. 6a).The curve shows type IV isotherm attended by H_3 type hysteresis loop. The analysis shows the existence of mesopores with specific surface areas of 2.11 $m^2\ g^{-1}$ of CTS material [38]. The charge intercalation is easily done through pore appeared at the surface of thin film. Hence, the conduction mechanism in the film is controlled by the pore size. The pore size distribution of the fine crystallites structure is built-in through Barrett-Joyner-Halenda (BJH) plot (see Fig. 6b). Figure 6b represents a curve of pore volume as a function of radius. Most of the pore volume is occupied by mesopores in the range of 3–50 nm.

4.9 Surface wettability study

The contact angle depends upon the chemical composition and the surface morphology of the semiconducting electrodes. In this study, the water contact angle is found to be 40, 29.8 and 21° for 0.526, 0.806 and 1.006 μm film thicknesses, respectively (see Fig. 7). From surface wettability study, it is observed that the interfacial energy between the film surface and water increased with thickness leads to decrease in contact angle. Surface wettability is decreased with increase in film thickness due to two reasons: (a) thick film has relatively less internal and external strain energies compared to the thin one [39] and (b) the contact angle decreases with roughness of the film surface [40].

4.10 Optical analysis

The optical absorption of CTS thin films for different thicknesses has been investigated as shown in Fig. 8a–c. The band gap energy of CTS thin films was calculated using the optical absorption spectroscopy. These spectra revealed that the deposited CTS thin films have high

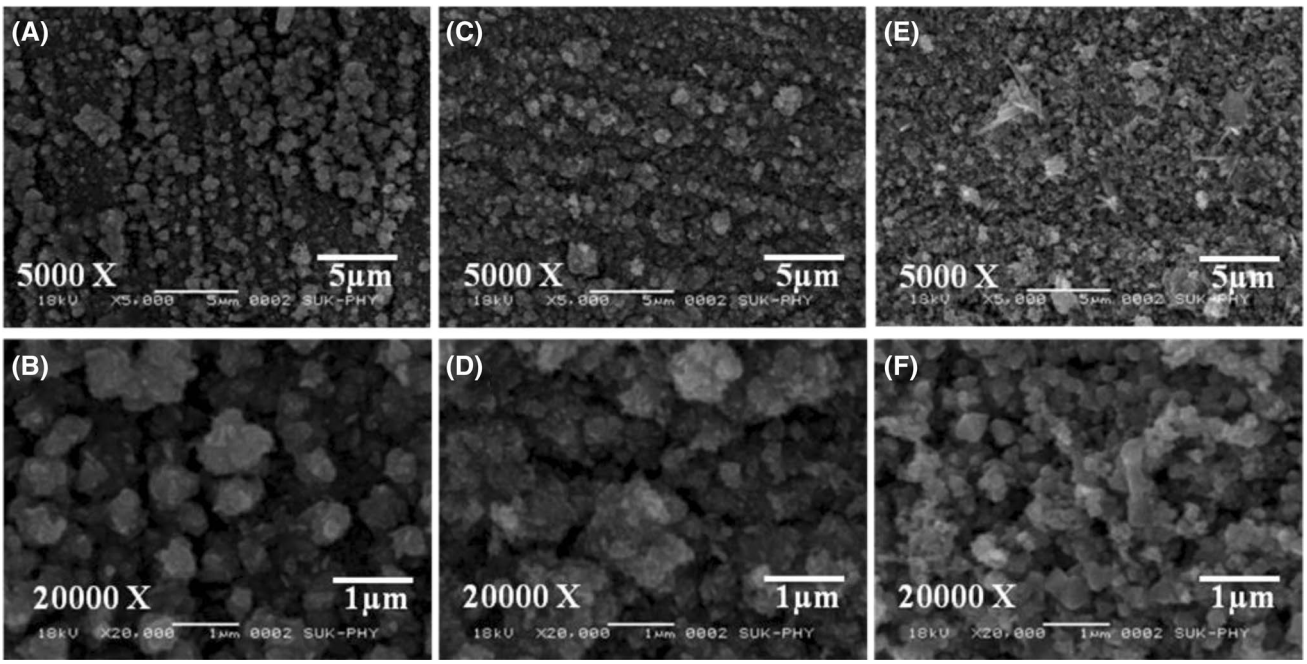

Fig. 5 SEM images of CTS-20 (**a, b**), CTS-40 (**c, d**) and CTS-60 (**e, f**) at two magnifications of ×5000 and ×20,000

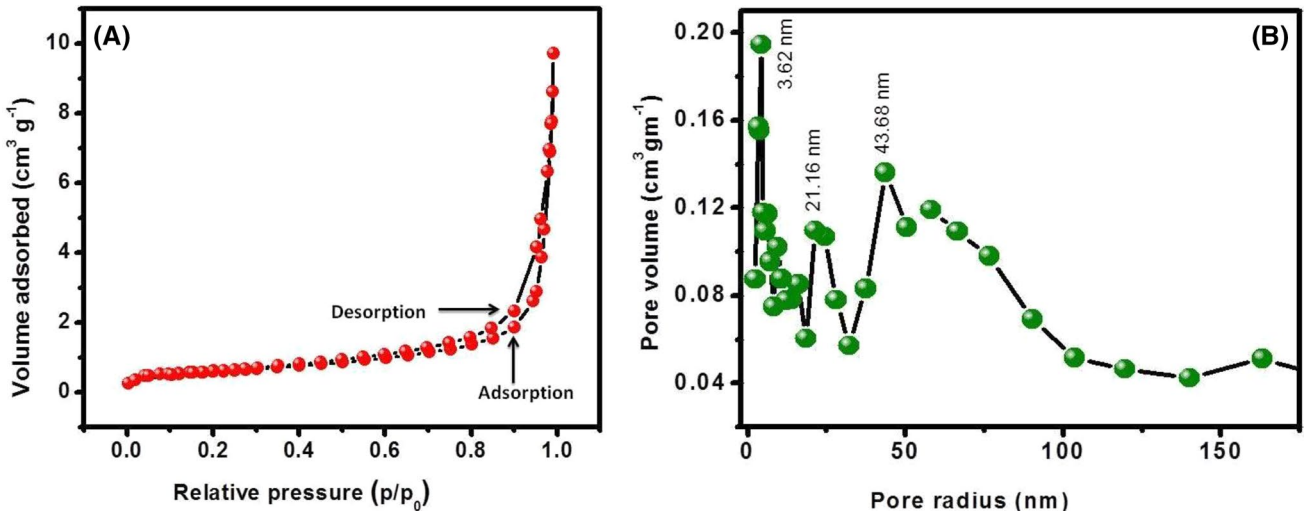

Fig. 6 **a** N_2 adsorption–desorption isotherm curve and **b** pore size distribution of Cu_2SnS_3 material

absorbance of light in the visible region, indicating its applicability as an absorbing material. Band gap values are estimated by plotting graph of $(\alpha h\upsilon)^2$ vs $(h\upsilon)$, where α is the absorption coefficient and hυ is the photon energy. The band gap (E_g) values are found to be 1.36, 1.18, and 0.98 eV for CTS-20, CTS-40 and CTS-60 films, respectively. It is observed from Fig. 8, that the band gap gradually decreases from 1.36 to 0.98 eV with the increasing film thickness. The decrease in band gap can be ascribed to the presence of secondary (CuS and SnS) phases in the compound as confirmed from the Raman study. Also from the compositional study, the Cu/Sn ratio increases from 2.17 to 2.49 with increasing film thickness. This increased copper composition results in absorbance of the light from the visible to IR region. Thus, the copper rich composition in the CTS compound leads to formation of secondary phase and eventually affects the band gap of the compound. Similar

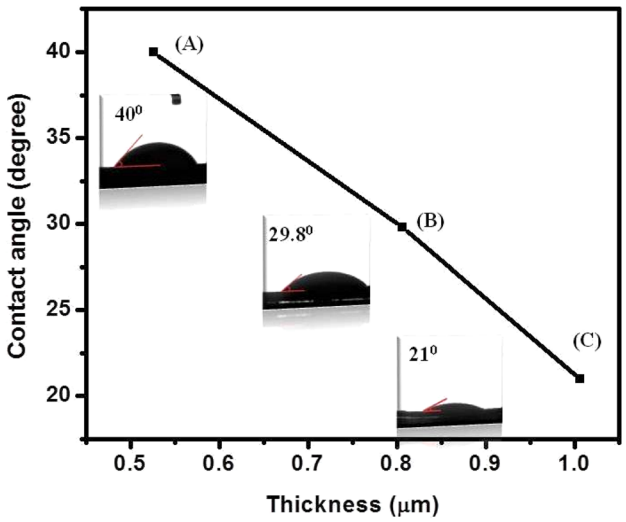

Fig. 7 Plot of surface wettability analysis of CTS thin films with film thickness. (*Inset* contact *angle* images of CTS material)

effect of band gap reduction from 2.19 to 1.77 eV for CTS films due to presence of secondary phases was observed by Zhao and Cheng [41].

4.11 Photo electrochemical measurement

Figure 9a–f shows the current–voltage (I–V) characteristics recorded under chopped and constant illumination conditions for CTS thin films of various thicknesses in 0.25 M $LiClO_4$ (Lithium perchlorate) electrolyte solution. The photovoltaic output characteristics of CTS thin films are studied by fabricating SS/CTS/LiClO4/C Cell. Gradually increasing anodic photocurrent with increase in negative potential indicates p-type conductivity of CTS thin film [42]. The magnitude of short circuit current (I_{sc}) is 77, 60.7 and 554 μA and open circuit voltage (V_{oc}) is 146, 30 and 216 mV for CTS-20, CTS-40 and CTS-60, respectively. The best PEC performance is obtained for CTS-60 thin film (Fig. 9e, f).

Solar cell parameters for CTS films of different thicknesses tabulated in Table 2 shows that sample CTS-60 represents better PEC performance. The highest values of photo conversion efficiency 0.11% with fill factor of 49% are achieved by CTS-60 thin film. As discussed earlier (Fig. 5), that the level of compact surface enhances slightly with the film thickness, which is useful for PEC properties. The PEC measurement confirmed good photoactivity of different thicknesses CTS thin films, prepared by simple SILAR method. Furthermore, the conversion efficiency of such film can be considerably increased by thermal, chemical and (photo) electrochemical surface treatments [43].

4.12 Conclusions

In conclusion, CTS thin films have been successfully deposited by simple and inexpensive SILAR method at room temperature. The effect of CTS film thickness on the structural, morphological and optical properties of CTS thin film is studied. The XRD studies revealed that CTS exhibit nanocrystalline structure with triclinic phase. Also, additional peak corresponding to secondary CuS phase is observed in the diffraction pattern. Improvement in crystallinity of the films with increasing film thickness was observed. Raman study confirms the formation of CTS compound with secondary CuS and SnS phases. The chemical composition of the films shows the presence of Cu, Sn and S in stoichiometric amount with slightly copper rich content (Cu/Sn = 2.17–2.49). The morphological study revealed that uniform, density and compact nature of the films increased with increasing film thickness. Also, with increasing CTS film thickness, optical band gap reduced which is related to enhancement

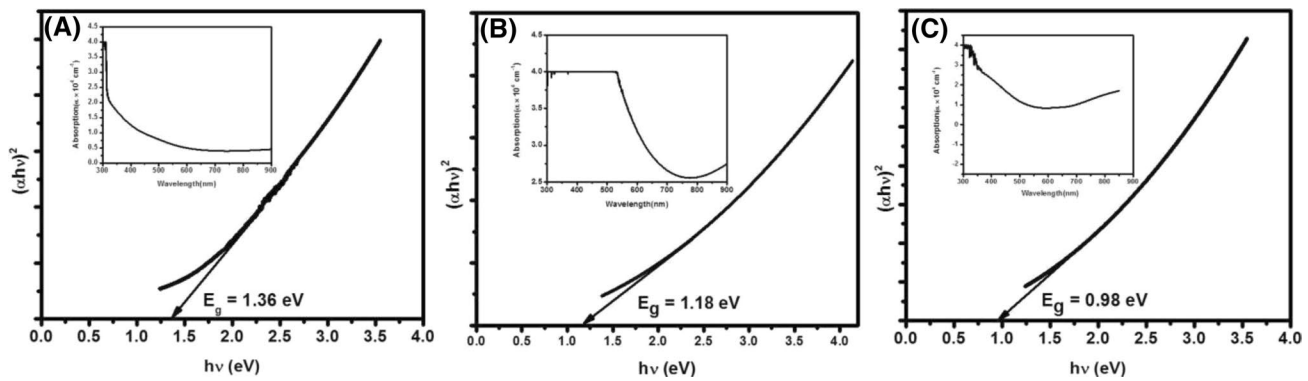

Fig. 8 Band gap plots and optical absorption spectra of **a** CTS-20. **b** CTS-40 and **c** CTS-60 thin films

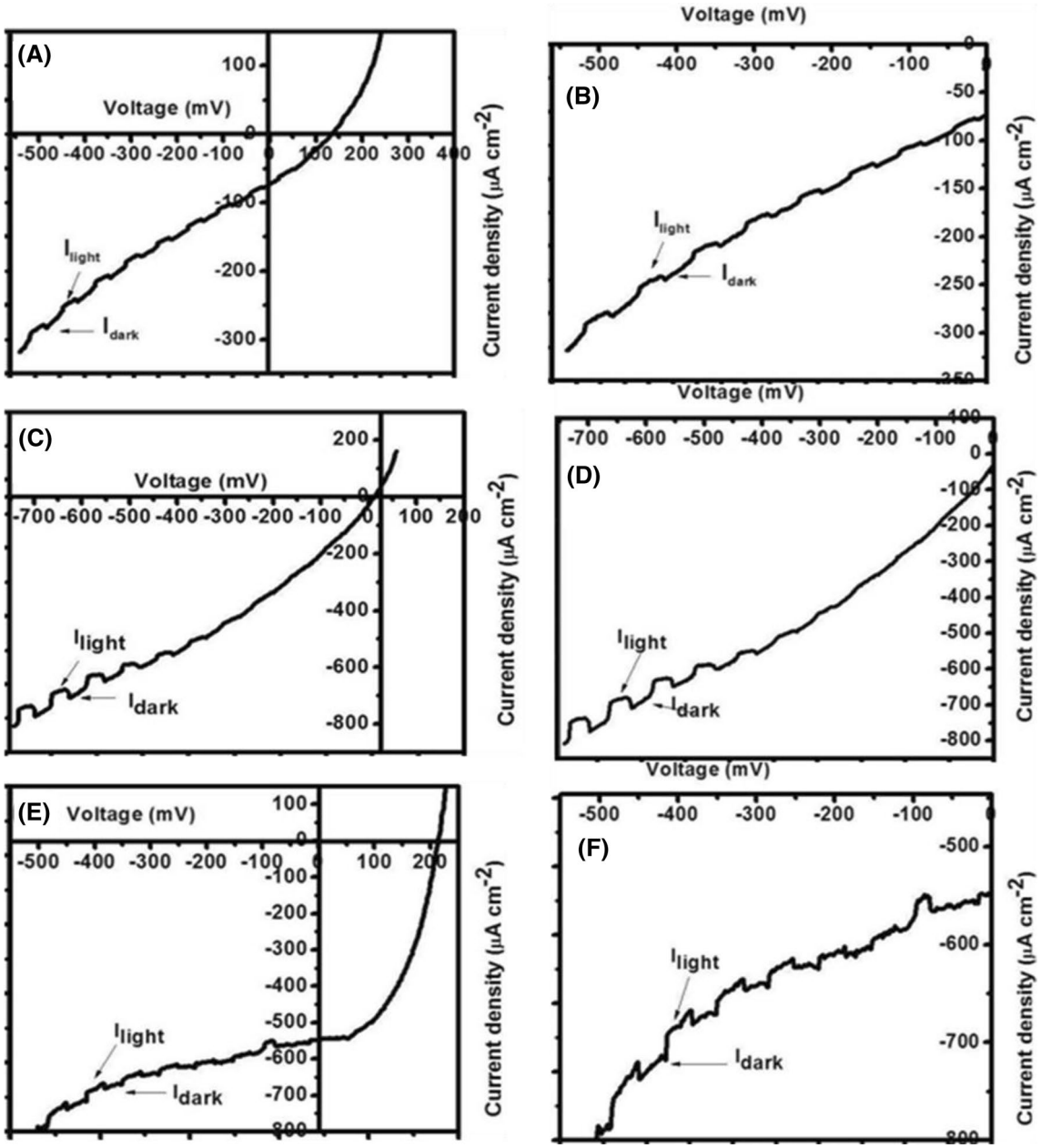

Fig. 9 Photovoltaic output characteristics of CTS-20 (**a, b**), CTS-40 (**c, d**) and CTS-60 (**e, f**) for different thicknesses CTS thin films under chopped light illumination with bias of (0.3) to (−0.5 V)

Table 2 Photoelectrochemical cell parameters of CTS materials

Sample	Thickness (μm)	I_{sc} (μA)	V_{oc} (mV)	I_m (μA)	V_m (mV)	FF %	η%
CTS-20	0.526	77	146	43.5	80.5	31	0.070
CTS-40	0.806	47.7	30	30.4	14.5	23	0.088
CTS-60	1.006	554	216	411	144.5	49	0.110

in the crystallite size and decrease in defect density of the film. The study of PEC properties confirms good photoactivity for sample CTS-60 having 1.006 μm thicknesses. Hence, it can be concluded that the film thickness plays an important role in performance of PEC cells and on the characteristic parameters of the films.

Acknowledgements Present work was supported by the Human Resources Development program (No.20124010203180) of Korea Institute of Energy Technology Evaluation and Planning (KETEP) Grant funded by the Korea government Ministry. The basic Science Research Program through the National Research Foundation of Korea (NRF) funded by the Ministry of Science, ICT (NRF2015R1A2A2A01006856).

References

1. J. Tang, S. Hinds, S. Kelley, E. Sargent, Chem. Mater. **20**, 6906–6910 (2008)
2. B. Shin, O. Gunawan, Y. Zhu, N. Bojarczuk, S. Chey, S. Guha, Prog. Photovolt Res. Appl. **21**(1), 72–76 (2013)
3. D. Barkhouse, O. Gunawan, T. Gokmen, T. Todorov, D. Mitzi, Prog. Photovolt Res. Appl. **20**, 6–11 (2012)
4. L. Baranowski, K. McLaughlin, P. Zawadzki, S. Lany, A. Norman, H. Hempel, R. Eichberger, T. Unold, E. Toberer, A. Zakutayev, Phys. Rev. Appli. **4**, 044017(1)–044017(9) (2015)
5. M. Adelifard, M. Mohagheghi, H. Eshghi, Royal Swedish Acad. Sci. Physica Scripta **85**, 035603–035608 (2012)
6. P. Fernandes, P. Salome, A.D. Cunha, J. Phys. D Appl. Phys. **43**, 1–11 (2010)
7. Z. Tang, K. Kosaka, H. Uegaki, J. Chantana, Y. Nukui, D. Hironiwa, T. Minemoto, Phys. Status Solidi (A), **212**, 2289–2296 (2015)
8. N. Aihara, A. Kanai, K. Kimura, M. Yamada, K. Toyonaga, H. Araki, A. Takeuchi, H. Katagiri, J. Appl. Phys. **53**, 08KC06(1)–08KC06(4) (2014)
9. U. Chalapathi, Y. Jayasree, S. Uthanna, V. Sundararaja, Vacuum **117**, 121–126 (2015)
10. T. Reddy, R. Amiruddin, M. Santhoshkumar, Sol. Energy Mat. Sol. Cells **143**, 128–134 (2015)
11. Y. Miyata, S. Nakamura, Y. Akaki, Phys. Status Solidi (C), **12**, 765–768 (2015)
12. X. Chen, H. Wada, A. Sato, M. Mieno, J. Solid State Chem. **139**, 144–151 (1998)
13. R. Ettlinger, A. Cazzaniga, S. Canulescu, N. Pryds, J. Schou, Appl. Surf. Sci. **336**, 385–390 (2015)
14. S. Vanalakar, G. Agawane, A. Kamble, C. Hong, P. Patil, J. Kim, Sol. Energy Mat. Sol. Cells **138**, 1–8 (2015)
15. M. Nakashima, J. Fujimoto, T. Yamaguchi, M. Izaki, Appl. Phys. Express. **8**, 04ES08(1)–04ES08(6) (2015)
16. A. Crovetto, R. Chen, R. Ettlinger, A. Cazzaniga, J. Schou, C. Persson, O. Hansen, Sol. Energy Mater. Sol. Cells **154**, 121–129 (2016)
17. B. Taher, M. Alias, I. Naji, H. Alawadi, A. Douri, Aust. J. Basic Appl. Sci. **9**, 406–411 (2015)
18. J. Han, Y. Zhou, Y. Tian, Z. Huang, X. Wang, J. Zhong, Z. Xia, B. Yong, H. Song, J. Tang, Front Optoelectron **7**, 37 (2014)
19. M. Shawky, A. Shenouda, El.. Said, I. Ibrahim, Int. J. Sci. Engg. Res. **6**, 1447 (2015)
20. D. Berg, R. Djemour, L. Gutay, G. Zoppi, S. Siebentritt, P. Dale, Thin Solid Films **520**, 6291–6294 (2012)
21. Z. Su, K. Sun, Z. Han, F. Liu, Y. Lai, J. Li, Y. Liu, J. Mater. Chem. **22**, 16346–16352 (2012)
22. G. Ilari, C. Fella, C. Ziegler, A. Uhl, Y. Romanyuk, A. Tiwari, Sol. Energy Mat. Sol. Cells **104**, 125–130 (2012)
23. A.C. Lokhande, K.V. Gurav, Eunjin Jo, Mingrui He, C.D. Lokhande, Jin Hyeok Kim, Opt. Mater **54**, 207–216 (2016)
24. F. Chen, J. Zai, M. Xu, X. Qian, J. Mater. Chem. **A1**, 4316–4326 (2013)
25. G. Hodes, *Chemical Solution Deposition of Semiconductor Films*. (Marcel Dekker, New York, 2005)
26. A. Lundin, G. Kitaev, Inorg. Mater. **1**, 1900–1905 (1965)
27. S. Kahraman, M. Podlogar, S. Bernik, H. Guder, Metall. Mater. Trans. A. **45A**, 2326–2334 (2014)
28. R. Salunkhe, D. Dhawale, T. Gujar, C. Lokhande, Mater. Res. Bull. **46**, 5009–5015 (2009)
29. V. Ashith, K. Rao, Thin Solid Films **616**, 197–203 (2016)
30. R.G. Pearson, Hard and soft acids and bases, HSAB, part1: fundamental principles, J. Chem. Educ. **45**(9), 295–310 (1968)
31. B. Strohmeier, D. Levden, R. Field, D. Hercules, J. Catal. **94**, 2806–2808 (1985)
32. R. Scheer, H. Lewerenz, J. Vac. Sci. Technol. A **12**, 56–60 (1994)
33. D. Tiwari, T. Chaudhuri, T. Shripathi, U. Deshpande, V. Sathe, Appl. Phys. A **117**, 1139–1146 (2014)
34. P. Grutsch, M. Zeller, T. Fehlner, Inorg. Chem. **12**, 1431 (1976)
35. A. Lokhande, K. Gurav, E. Jo, M. He, C. Lokhande, J. Kim, Opt. Mater. **54**, 207–216 (2016)
36. U. Jadhav, S. Patel, R. Patil, Res. J. Mater. Sci. **1**, 21–25 (2013)
37. M. Saglam, A. Ateş, B. Guzeldir, O. Ozakın, Phys. Status Solidi (A), **209**, 687–693 (2012)
38. Y. Akaltun, M.A. Yıldırım, A. Ates, M. Yıldırım, Opt. Commun. **284**, 2307–2311 (2011)
39. A. More, J. Gunjkar, C. Lokhande, R. Mane, S. Han, Micron **38**, 500–504 (2007)
40. G. Palasantzas, J. Hosson, Acta Mater. **49**, 3533–3538 (2001)
41. K. Zhao, H. Cheng Adv. Mater. Sci. Eng., **203**, 1–4 (2013)
42. Y. Chen, C. Chuang, K. Lin, S. Shen, C. McCleese, L. Guo, C. Burda, J. Phys. Chem. C **118**, 11954–11963 (2014)
43. D. Brion, Appl. Surf. Sci **5**, 133–152 (1980)